2014

Field Tests and Numerical Modeling of Vehicle Impacts on a Boulder Embedded in Compacted Fill

Lynsey Reese
Pennsylvania State University, ldr144@psu.edu

Tong Qiu
Pennsylvania State University, tqiu@engr.psu.edu

Daniel Linzell
University of Nebraska-Lincoln, dlinzell@unl.edu

Edward O'Hare
Pennsylvania State University, evo101@psu.edu

Zoltan Rado
Pennsylvania State University, zrado@engr.psu.edu

Field Tests and Numerical Modeling of Vehicle Impacts on a Boulder Embedded in Compacted Fill

Lynsey Reese[1], Tong Qiu[2*], Daniel Linzell[3], Edward O'Hare[4] and Zoltan Rado[5]

[1]PhD Candidate, Department of Civil and Environmental Engineering, The Pennsylvania State University, University Park, PA 16802, USA. E-mail: ldr144@psu.edu

[2]Assistant Professor, Department of Civil and Environmental Engineering, The Pennsylvania State University, University Park, PA 16802, USA. E-mail: tqiu@engr.psu.edu

[3]Voelte-Keegan Professor, Department of Civil Engineering, The University of Nebraska-Lincoln, Lincoln, NE 68588, USA. E-mail: dlinzell@unl.edu

[4]PhD Candidate, Department of Civil and Environmental Engineering, The Pennsylvania State University, University Park, PA 16802, USA. E-mail: evo101@psu.edu

[5]Senior Research Associate, The Thomas D. Larson Pennsylvania Transportation Institute, The Pennsylvania State University, University Park, PA 16802, USA. E-mail: zrado@engr.psu.edu

Received on 19 March 2014, Accepted on 14 Oct 2014

ABSTRACT

Landscape Vehicular Anti-Ram (LVAR) systems are a group of protective barriers, which are designed using natural materials (e.g., boulders) and have proven to both effectively protect sensitive structures against threats and be aesthetically pleasing. This paper presents two consecutive vehicular crash tests hitting the same single boulder embedded in AASHTO coarse aggregate fill. A LS-DYNA model was developed to simulate the field-scale tests, which were instrumented with high-speed cameras and pressure cells. A readily available truck model from the National Crash Analysis Center was modified and implemented in the LS-DYNA model. The boulder and surrounding soil were modeled using the Mohr-Coulomb failure criteria. The model parameters were calibrated using results from the first field-scale test with a truck traveling at 48.3 km/hr (30 mph) impacting the LVAR system. The calibrated model was then used to simulate the second field-scale test, which involved a truck traveling at 80.5 km/hr (50 mph) impacting the same LVAR system without resetting the boulder or soil. The calibrated model was able to provide the global response of the system, including the time-history of the translational displacement and rotation of the boulder, and was in good agreement with field-

*Corresponding author: tqiu@engr.psu.edu

scale test results. This suggests that the overall global response was dominated by the dynamic behavior of the truck and boulder system upon impact. Hence, a simple material model for soil and boulder is sufficient for simulating the tests conducted.

Key words: anti-ram systems, boulder, crash tests, field-scale tests, numerical modeling, soil-structure interaction

1. INTRODUCTION

The development of perimeter barriers has become critical for protecting buildings and facilities against vehicular impacts. Landscape Vehicular Anti-Ram (LVAR) systems are a group of protective barriers that effectively protect against threats using natural materials (e.g., boulders) and, as a result, can be aesthetically pleasing. Typical bollard systems are a collection of anti-ram barriers that typically use bollards with a deep, stiff foundation to achieve a proper standoff distance. The development process of these systems includes field-scale testing and numerical modeling to effectively design and validate these systems subjected to vehicular impacts. Field-scale tests involve using medium-duty trucks for vehicular impacts into these systems to validate each of the systems designed based on numerical modeling. Abundant field-scale testing and numerical modeling have been conducted on typical bollard systems [1–7]; however, limited research exists for LVAR systems [8].

In order to adopt a unified test method to test the crashworthiness of vehicle barriers such as anti-ram devices, the U.S. Department of State (DOS) established a standard for device designs, the *Specification for Vehicle Crash Test of Perimeter Barriers and Gates* (SD-STD-02.01) [9] in 1985. SD-STD-02.01 specified preliminary criteria related to the test vehicle (diesel or gas engine medium-duty truck (6800 kg)), ballast attachment, impact velocity and penetration distance. With the use of small-sized cars in more recent terrorist attacks, the American Society for Testing and Materials (ASTM) established a new standard–*Standard Test Method for Vehicle Crash Testing of Perimeter Barriers* (F2656-07) [10]. This test method provides a structured procedure to establish a penetration rating for perimeter barriers subjected to vehicle impact as well as site condition requirements during installation and testing and standard vehicular energy requirements. ASTM F2656-07 test standards have been used in numerous research projects including those tested at the Larson Transportation Institute [1, 2, 8] and the Texas Transportation Institute [11].

Numerical modeling of anti-ram barrier systems has been generally conducted using LS-DYNA [12], which is known to be a reliable program for modeling vehicular impact and contains a library of constitutive models developed for high-strain-rate loads for a number of materials. LS-DYNA also has several different contact formulations that are effective in high-strain-rate impacts including single-surface, one- and two-way contacts. These common contact formulations accurately maintain compatibility between parts within the model. Numerous researchers have investigated typical bollard systems using LS-DYNA as a means to validate field-scale tests [1–7]. O'Hare et al. [1] developed Streetscape Vehicular Anti-Ram (SVAR) systems with shallow foundations, including street benches, bus stops and street signs, which were able to conform to site restrictions, use cost effective standard materials, and accommodate varying architectural aesthetics. The design of the SVAR systems was optimized using LS-DYNA and then validated through field-scale testing. Other researchers validated DOS standard impact conditions for anti-ram bollards known as K4, K8,

and K12 through field-scale testing; using LS-DYNA, researchers were able to offer recommendations and modifications for each of the barriers after validation since the model simulations predicted the standard impact conditions [3].

Research conducted at the Larson Transportation Institute, affiliated with the Pennsylvania State University, on the design and performance of a LVAR system consisting of a boulder embedded in compacted fill will be summarized herein. Two field-scale tests were conducted and used to rate the performance of barrier systems against M30 (vehicular speed of 48.3 km/hr (30mph)) and M50 (vehicular speed of 80.5 km/hr (50mph)) impacts. Due to minimal movement of the boulder and displacement of the surrounding soil at M30, a M50 test was conducted to assess the performance of the system at a higher vehicular impact velocity without replacing the boulder or surrounding soil. Using high-speed cameras, pressure cells, and field surveys the boulder movement and soil pressure were obtained from each test. A LS-DYNA model was developed to predict the overall global response of the system to vehicular impact and the simulated results were compared to the collected field data. In the following sections, the field-scale tests are first described followed by descriptions of the LS-DYNA model and selection of model parameters. Lastly, results and discussions on the capability of the LS-DYNA model in capturing global response of the LVAR system are presented. This paper focuses on the numerical predictions and measured performance for a LVAR system in the field-scale. The results therefore provided a useful basis for evaluating the predictive capabilities and limitations of the numerical analyses.

2. FIELD-SCALE TESTING

Vehicular impact tests were conducted according to ASTM F2656-07 - Standard Test Method for Vehicle Crash Testing of Perimeter Barriers [10], which establishes a penetration rating for perimeter barriers subjected to a vehicular impact. The test facility uses a rigid rail to provide vehicle guidance, a reverse towing system to accelerate the test vehicle to the required speed, and a release mechanism that disconnects the tow cable and steering guidance prior to impact. The propulsion system used to bring the test vehicle up to the desired impact speed consists of a tow vehicle, a tow cable, two re-directional pulleys anchored to the ground, a speed multiplier pulley attached to the tow vehicle, a quick-release mechanism, and a ground anchor. For a detailed description of the system, please refer to Reese et al. [8].

Two consecutive, full-scale field tests were conducted and consisted of the same Rockville White (RW) granite boulder embedded in AASHTO uniformly-graded coarse aggregate soil. Test 1 was for a M30 impact while Test 2 was for a M50 impact. In between these tests, the RW granite boulder was not reset and surrounding soil was not recompacted. Field surveys were completed before and after each test to determine the final displacement of the boulder and each truck.

The test vehicles used in this study were medium-duty diesel trucks. The truck used in Test 1 was a 1999 International 4700 single-unit flatbed truck. Barrels with ballast were secured on the bed of the truck making the test inertia weight 6745 kg. The height to the lower edge of the front bumper was 0.48 m and the height to the upper edge of the front bumper was 0.75 m. The second truck used was a 1999 International 4700 single-unit flatbed truck. Test inertia weight of the vehicle was 6827 kg. The height to the lower edge of the front bumper was 0.48 m and the height to the upper edge of the front bumper was 0.76 m.

According to ASTM F2656-07 (2007) standards, during the installation of the RW boulder, the excavation should extend along the horizontal direction behind the boulder to a distance equal to 1.5 times the boulder embedment depth [10]. As shown in Figure 1, this

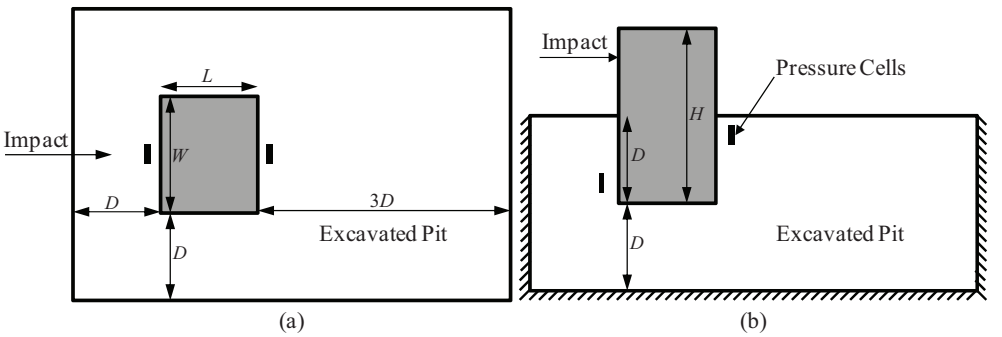

Figure 1. General layout for field test configuration: (a) plan view; and (b) elevation view (Dimension of excavated pit to scale, Dimension of boulder is not to scale)

criterion is satisfied. Prior to each test, the extent of excavation was surveyed and the geometry was utilized as an input parameter for the numerical simulations to be discussed later. Prior to boulder placement, the AASHTO uniformly-graded coarse aggregate soil was placed into the excavated pit to the desired elevation in lifts of approximately 0.2 m and compacted using a tamping compactor. The boulder was then lowered into the pit and centered for the impact. Similar procedures were followed to backfill the pit with compacted aggregates.

The RW granite boulder was approximately 1.98 m wide (W) × 1.68 m long (L) × 3.43 m high (H) as shown in Figure 1. The total embedment depth (D) was 2.03 m. The approximate weight of the boulder was 27,200 kg. No natural fissures or joints were observed in the boulder. Based on the information provided by the quarry, the bulk density and compressive strength of the boulder were approximately 2696 kg/m^3 and 142 MPa, respectively [13]. Small-scale testing was completed to confirm these values and will be briefly discussed in a subsequent section.

The field tests were instrumented with high-speed cameras to record the motions of the truck and boulder immediately prior to and after the crash and pressure cells were embedded in the soil to monitor pressure variations during the tests. The high-speed camera systems are fully autonomous and can capture images up to 29,000 frames-per-second with a maximum resolution of 1016 × 1016. Three cameras (see Figure 2) were used during each test and they

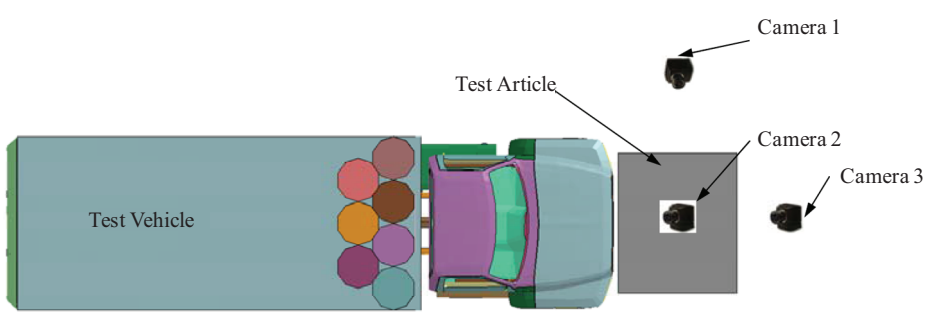

Figure 2. Location of high-speed video cameras during field test (not to scale)

Figure 3. Still images from high-speed camera 1 at: (a) t = 0 sec; (b) t = 0.1 sec; (c) t = 0.2 sec; and (d) t = 0.3 sec

were positioned (1) at a 90° angle and 20.5 meters to the center of the test article to measure dynamic penetration; (2) at a 90° angle and 15.9 meters above the center of the test article to capture enough surface area prior to and after impact to determine impact speed, impact angle, exit angle and debris field; and (3) behind the test article at a distance of 32.2 meters centered along the guidance rail to record the approach of the test vehicle to track its alignment with respect to the center of the test article. Specific points on the impacted system were tracked using fiducials that allow tracking of critical points during impact. High-speed video and still images from Camera 1 were utilized to determine boulder movement time history for comparison with LS-DYNA simulations. Figure 3 represents two tracking fiducials and still images at different stages of impact for Test 1.

Hydraulic-type pressure cells [14] were embedded inside the compacted aggregates to monitor earth pressure time histories at the front and back of the boulder during each impact. The cells use two flat plates, welded together at their periphery, and are separated by a small gap filled with a fluid. When a load is applied to the cell, the hydraulic fluid is squeezed between the two plates and a pressure build occurs with the change in pressure being

converted to an electric signal. The resulting pressure-time histories can provide insight into the dynamic soil-boulder response upon impact and are utilized for numerical comparison to LS-DYNA simulations. General locations of the pressure cells are shown in Figure 1.

3. LS-DYNA MODEL

The LS-DYNA [12] research/commercial code was utilized to perform Finite Element Method (FEM) simulations to model the vehicular impact tests. This code was chosen due to its proven capability in modeling impact events [1, 3, 6, 8, 11]. The FEM model is shown in Figure 4, which details the different mesh densities used for the truck, boulder, and soil domain. This section will briefly discuss the truck, boulder, and soil constitutive models used in the numerical simulation as well as stress initializations used to simulate the initial condition of both tests under gravity loading and the initial condition of the M50 test after the M30 impact.

3.1. TRUCK MODEL

Field-scale frontal impact tests against anti-ram barriers have indicated that a truck typically absorbs approximately 70% of the impact energy for a M30 rated test [3]. Therefore, a realistic truck model that can capture the correct amount of energy absorption during an impact event is essential. The truck model used for the simulations, shown in Figure 4, was modified from a model readily-available in the National Crash Analysis Center (NCAC) database [15, 16]. The FEM model was based on a 1996 Ford F800 single unit truck as shown in Figure 5(a) and was developed to meet the needs of roadside hardware research and development community while reducing computational requirements. The NCAC truck model was developed to ensure that the load transfer between the truck and hardware, the deformation of the truck, and the overall behavior of the truck during impact simulations would be as accurate as feasible given the model computational requirements.

The truck requirement for ASTM F2656-07 is a Ford F650 or Ford F750, which was different than the NCAC truck model. Field-scale tests, however, utilized a flatbed medium duty truck with ejectable added cargo mass in the form of 55-gallon barrels filled with ballast and secured towards the front of the truck's bed with ratchet straps. Modifications to the

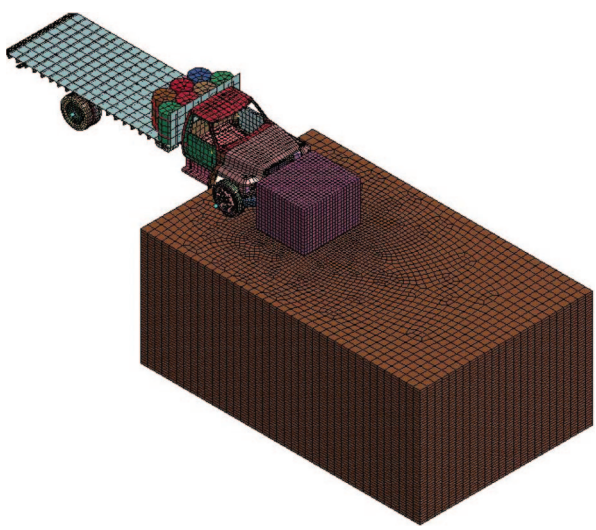

Figure 4. LS-DYNA FEM truck/boulder/soil numerical model

Figure 5. FEM truck model modifications: (a) NCAC truck model; and (b) Modified truck model

truck model, as shown in Figure 5(b), were needed to meet the criteria of the standard. Joint revolution constraints were added to allow the wheels to rotate and truck ramping. The closed bed on the original truck was removed, leaving an open truck bed for the added ballast barrels. The ballast barrels were added to meet the required weight according to ASTM F2656-07. An accelerometer was added at mass center of the truck to monitor the response time history to compare vehicle dynamics from field-scale tests and numerical simulations. Last, definitions of conservative failure strains for all truck's materials were added to prevent unrealistic energy absorption due to extreme deformation.

The modified truck model consisted of 1606 eight-node constant stress solid elements, 20,318 four-node Belytschko-Tsay shell elements and 201 Hughes-Liu with cross section integration beam elements. Three validation checks and visual comparison to field-scale Test 1 were conducted to ensure the modified truck model could capture the global response of the ASTM-specified truck under impact [17, 18]. First, the truck model was validated using checks of equilibrium by preloading the truck with a gravity load using LS-DYNA. The normal force on the rigid floor beneath the truck was then compared to the weight of the truck to ensure the mass of the truck satisfied ASTM F2656-07. Second, energy conservation was checked to ensure that excessive internal energy, such as hourglass energy, did not contribute to spurious numerical results as shown in Figure 6. The figure

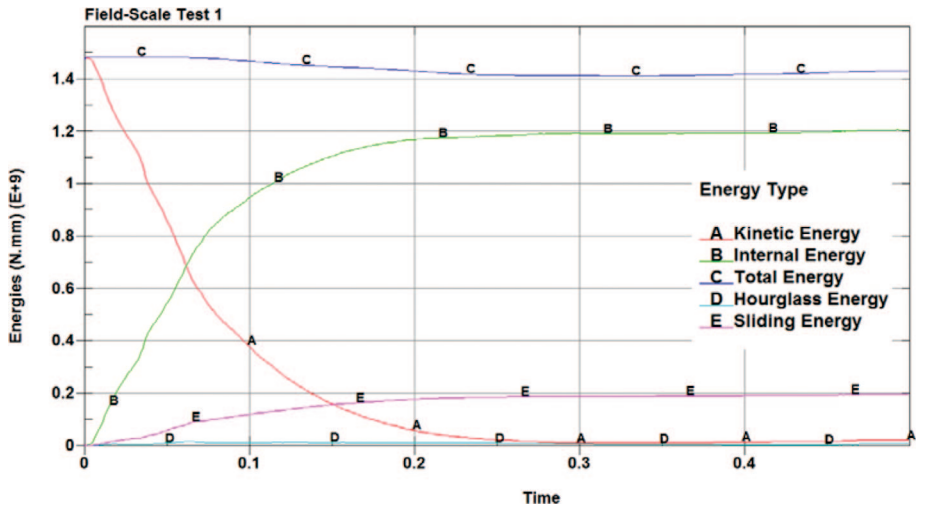

Figure 6. Energy balance diagram for field-scale Test 1

shows a relatively constant energy suggesting that there are no unusual characterizations in the structure of the model that would result in unrealistic dissipation of energy. Sliding energy, associated with friction between the truck and barrier, also increases during the simulations. Third, using the numerical simulation from Test 1 (speed of 48.3 km/hr), the ratio of the internal energy of the truck after impact to the initial energy of the system (i.e., kinetic energy of the truck) indicated that the truck absorbed approximately 69% of the impact energy, which is consistent with the field-scale test conducted by Omar et al. [3]. The absorbed energy is due to plastic deformation and fracturing of various truck components. Lastly, Figure 7 provides a visual comparison of the simulation versus field-scale Test 1. This sequential view shows that there was similar behavior of the vehicle for each of the time steps shown.

3.2. CONSTITUTIVE MODEL FOR BOULDER AND SOIL

The LS-DYNA Material Type 173, "Mohr-Coulomb (M-C)" [12, 19] was utilized to model the boulder and soil behavior in the FEM simulations. The M-C model was used to represent the soil and boulder due to its ability to effectively and simplistically capture impact conditions present in the field testing. Although the M-C constitutive model is simple and cannot capture sophisticated post-failure constitutive behaviors such as the strain softening response and fracture propagation, it is considered sufficient to model the boulder behavior during the field tests as no damage to the boulder was observed and it essentially behaved as a rigid mass. The M-C model is also considered sufficient in modeling the constitutive behaviors of the compacted granular fill as small deformations of the fill were observed after the impacts. The Mohr-Coulomb characterizes failure of a material based on its cohesion, normal stress and friction angle as follows [12]:

$$\tau_{\max} = c + \sigma_n \tan(\phi) \tag{1}$$

where $\tau_{\max}$ is the shear strength on a plane, σ_n is the normal stress on that plane, c is cohesion and ϕ is the friction angle. Model parameters for the boulder and soil are discussed later.

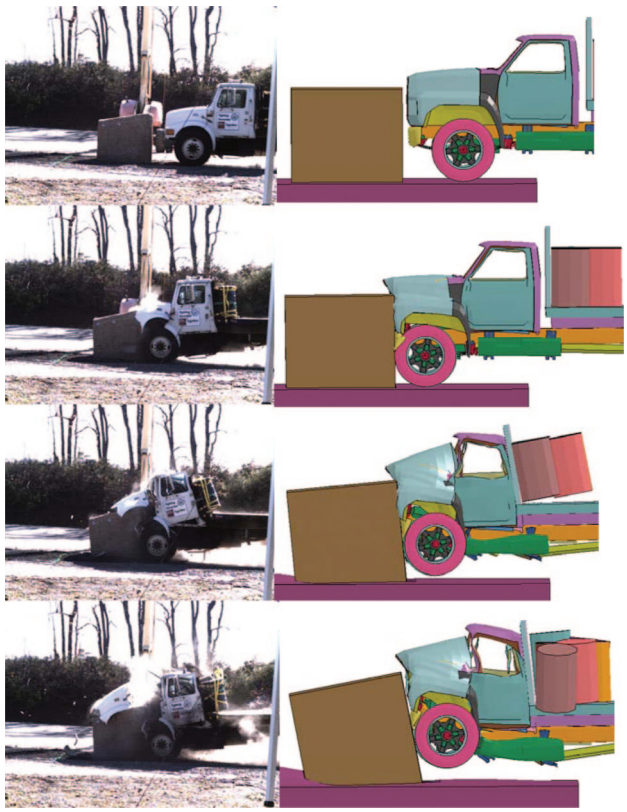

Figure 7. Sequential views comparing field-scale Test 1 to simulation results

3.3. PRELOAD AND STRESS INITIALIZATION

A springback analysis procedure readily available in LS-DYNA was utilized to preload the system with gravity so that the stress-dependent soil strength and conditions prior to impact were modeled correctly. Once a steady-state condition was reached, information from the model was outputted and used for all subsequent modeling using a sequential analysis. Pressure distributions in the soil with respect to depth and total body equilibrium from the steady-state condition were checked to ensure that gravity was applied correctly.

A stress initialization procedure in LS-DYNA was utilized to model consecutive impacts on the boulder that, as discussed earlier, occurred without resetting the boulder or recompacting the soil. For the simulation of Test 1, sufficient analysis time was utilized to allow the system to reach a steady-state condition. Then, pertinent information from the end of the simulation, which included the deformed geometry of the soil-boulder system, residual stress and strain patterns within the soil-boulder elements, and boundary conditions of the soil domain, was carried over to the beginning of the Test 2 simulation. An undeformed truck, using the Test 2 speed, was then used in the numerical model for the Test 2 simulation.

4. MODEL PARAMETERS

Data collected from Test 1, such as recorded boulder translations and rotations, were utilized to calibrate input parameters for the LS-DYNA model including constitutive parameters for the boulder and soil, contact algorithms, and domain size. Test 1 was chosen for calibration

due to the minimal rotational and translational movement of the boulder during impact. This section will discuss general parameters for contact algorithms used in the simulation, boulder material model to determine key parameters, and calibration of soil material parameters. The calibrated model is subsequently utilized to predict the global response of the LVAR system for Test 2 and compare with data collected from high-speed cameras and pressure cells.

4.1. BOULDER MODEL

Laboratory tests were conducted at CITEL to determine the RW boulder material properties for numerical simulation under different conditions (e.g., quasi-static and high-strain rates) that would be subsequently implemented into computational models. These tests included uniaxial compression, split tension, Chevron bend, split Hopkinson pressure bar tests, and Schmidt hammer [20–22]. Uniaxial compression tests determined the ultimate compressive strength; split tension tests measured the uniaxial tensile strength; Chevron bend tests determined the fracture toughness of rock material and its Young's modulus [20]. In addition to these quasi-static tests, split Hopkinson pressure bar (SHPB) tests were conducted to evaluate the rate effects of material behavior [21]. The Schmidt Hammer test was conducted in the field to quickly determine the compressive strength of rock material [22]. Based on the tests conducted an initial shear modulus of 9480 MPa was determined, which is consistent with typical properties of granite published in literature [23, 24].

The boulder domain was constructed using eight-node constant stress solid elements. Each element was 100 mm x 100 mm x 100 mm. This mesh size was selected to create a smooth transition from the boulder domain to the soil domain, which is described below, and also to create adequate nodal contacts between the two contact surfaces.

A single variant analysis was conducted to determine the sensitivity of the numerical simulation to the initial shear modulus (G) of the boulder, which demonstrates that the boulder displacement was relatively insensitive to the change of boulder stiffness. For example, Figure 8 shows the effect of changing the boulder's shear modulus by ± 25% on

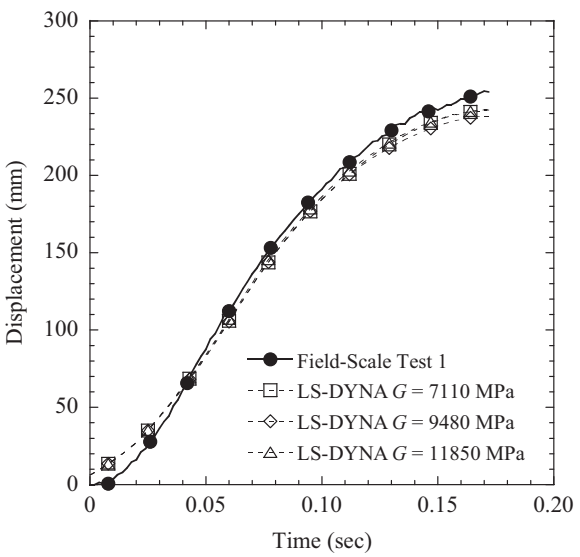

Figure 8. Effect of varying boulder elastic shear modulus on Test 1 center of gravity (C.G.) displacement

Table 1. Summary of boulder and soil parameters used in M-C model

	Density (tonne/mm^3)	Elastic shear modulus (MPa)	Poisson's ratio	Friction angle (degrees)	Cohesion (MPa)	Dilation angle (degrees)
Boulder	3.056×10^{-9}	9480	0.25	37.8	18.3	0
Soil	2.1×10^{-9}	20	0.25	45	0.0048	15

boulder displacement time history while keeping other parameters constant. Additional sensitivity analyses also confirmed that other global responses of the system (e.g., boulder rotation and truck penetration) are insensitive to the boulder's shear modulus. This is likely due to several reasons. First, the boulder's response was largely elastic during the field tests as no fracture of the boulder was observed after the tests. Second, the boulder rotation and displacement were likely governed by the surrounding soil, which has considerably lower stiffness and strength than the boulder. Consequently, the boulder essentially behaved as a rigid mass transferring the impact momentum and energy to the surrounding soil. The selected boulder properties were summarized in Table 1.

4.2. SOIL MODEL

The soil domain, representing the AASHTO uniformly-graded coarse aggregate, was constructed using eight-node constant stress solid elements. The extent of the soil domain needs to accurately predict the global response of the impact event. Since the impact event occurred over a short duration, the extent of the modeled soil domain does not need to be expansive as long as the reflected wave does not influence the simulation. Based on these considerations, the soil domain extends one embedment depth from the impact face, sides and beneath the boulder and three embedment depths behind the boulder as shown in Figures 1 and 4. This domain was computationally efficient and accurately predicted the global response. Boundaries of the modeled soil domain were constrained based on anticipated motion of each side of the exterior soil domain. For example, the sides of the soil domain (parallel and perpendicular to impact) were restrained against translation normal to their exterior surfaces and the bottom of the soil domain was restrained in the vertical direction. These imposed boundary conditions adequately constrained the soil domain when attempting to predict global response of the system because of the impact event's short duration.

In conjunction with model calibration, a sensitivity study was conducted to determine an optimal mesh density for the soil with respect to model accuracy and computational efficiency. The mesh transitioned from the highest mesh density (i.e., finest) near the boulder to the lowest density (i.e., coarsest) at the exterior of the soil domain as seen in Figure 4. This transition was based on anticipated distribution of strain intensity within the soil domain. To realistically model the soil as a continuum, each soil element should represent a sufficient number of soil particles, and, for the soil used in these tests (i.e., AASHTO uniformly-graded coarse aggregate), the smallest realistic soil element size was determined to be 50 mm in each local Cartesian direction based on the average aggregate size. A mesh sensitivity study was conducted to investigate the effect of the smallest element size of 50 mm, 75 mm, and 100 mm on the numerical simulation to determine the optimal mesh density near the boulder, where large displacements were anticipated, and to increase computational efficiency while maintaining an accurate global response of the system. Results of this parametric study indicate that the smallest element size of 75 mm provided optimum combination of accuracy and computational efficiency. The largest mesh density on the exterior of the soil domain remained

constant at 250 mm. Hence, the optimum mesh was determined to be 75 mm near the boulder-soil interface and smoothly transitioning to 250 mm at the exterior of the soil domain.

Calibration of the M-C constitutive parameters for the backfill soil was conducted based on the results of Test 1. These parameters included shear modulus (G), friction angle (ϕ), dilation angle (ψ), and cohesion (c). Based on the gradation and angularity of the AASHTO coarse aggregate the friction angle is estimated to be 45° and the dilation angle is estimated to be 15° [25]. A sensitivity analysis indicated that shear modulus and cohesion had a greater influence on the global response of the system than the friction and dilation angles. Figure 9 shows a comparison of simulated boulder displacement versus time based on varied values of G and c with recordings from Test 1. Figure 9 shows that the boulder translational displacement increases as the shear modulus of soil decreases. A combination of G = 20 MPa and c = 4.8 kPa yielded an excellent match with field-scale recordings. Hence, this combination was used for subsequent simulations. Table 1 summarizes material constitutive properties used in this study.

4.3. CONTACT ALGORITHMS

Contact algorithms were used to mimic frictional interaction between the boulder and soil, truck and LVAR system, and self-contact of truck components. One- or two-way contact sliding interfaces, which prevented nodes of selected elements from penetrating the surfaces of others, were used to represent boulder-to-soil and vehicle-to-LVAR barrier contact. The one-way formulation was checked to determine if the nodes of a defined slave part penetrated the surfaces of a defined master part while two-way formulation was checked for penetrations in both directions [19]. The static contact friction angle between the boulder and soil was selected to be 22.5° (i.e. 0.5*ϕ) [26] which gives a friction coefficient of 0.414. The dynamic coefficient of friction is assumed to be the same as the static coefficient. The static coefficient

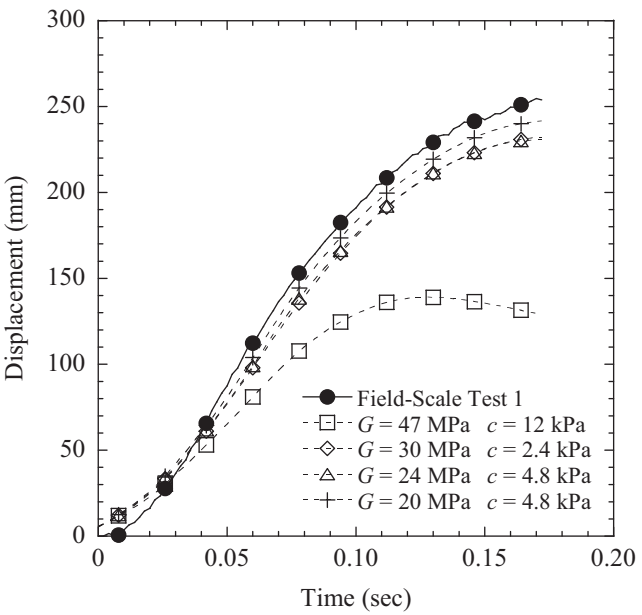

Figure 9. Effect of varying elastic shear modulus and cohesion on Test 1 C.G. displacement

of friction between the truck and LVAR system was 0.4 [1]. A standard penalty formulation that places interface springs normal to all penetrating nodes and contact surfaces was chosen to represent interaction between the truck and boulder because the stiffness of each was approximately in the same order of magnitude. A soft constraint penalty formulation, which calculates the stiffness of the interface springs based on stability considerations during a given time step, was chosen for contact between the boulder and soil due to large differences in their stiffness magnitudes [12]. These penalty-based formulations were useful because no special treatment of intersecting interfaces is required. In addition, this approach minimizes hourglassing that could potentially occur in elements representing the soil due to large deformations that are anticipated in the soil during the impact events [19].

5. RESULTS AND DISCUSSION

Two field-scale tests were conducted and used to rate the performance of LVAR barrier systems against M30 and M50 impacts. Using the data collected from the field and calibrated soil and boulder material models the results are discussed in the following section. The final position of the truck after impact from Test 1 and Test 2 and snapshots of their respective LS-DYNA simulations are shown in Figure 10. From this qualitative comparison, the only observed differences were that the truck hood detached in both field-scale tests and the barrels did not eject in Test 1 when compared against the simulation. The amount of truck deformation was very similar between the field-scale test and respective simulations. Quantitative investigations that follow revealed that these observed differences played a minor role in relation to overall performance and the LS-DYNA model was determined to have accurately predicted actual impact behavior.

Figure 11 presents a comparison of simulated boulder translational displacement versus time with test recordings based on fiducial tracking for Tests 1 and 2. Figure 12 shows the

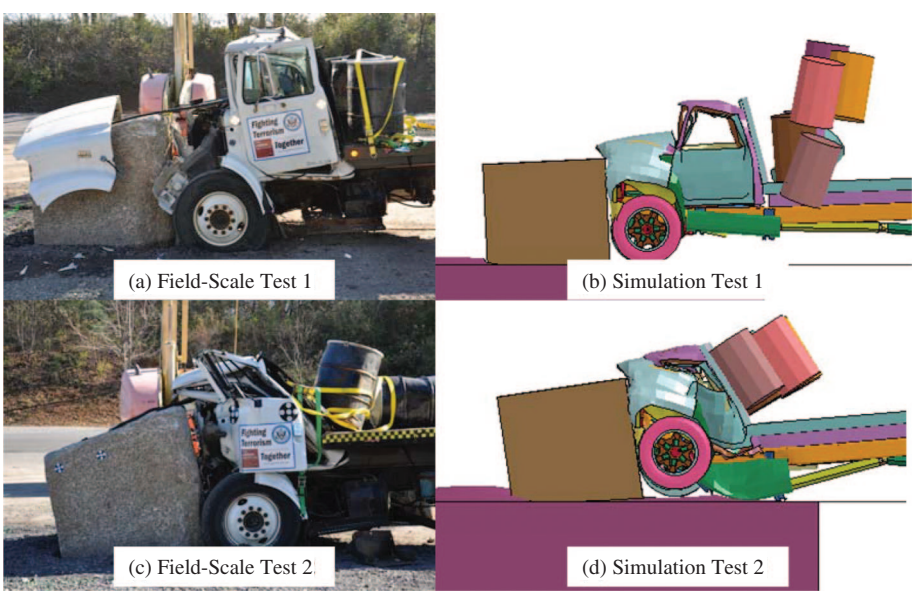

Figure 10. Comparison of final impact condition of field-scale tests and LS-DYNA simulations: (a) Field-Scale Test 1; (b) Simulation Test 1; (c) Field-Scale Test 2; and (d) Simulation Test 2

corresponding plot for boulder rotation. Both plots show good agreement between the test and simulation, although there is a slight disparity for boulder rotation in Test 2. This disparity was attributed to soil particles in the numerical simulation unable to fill the void created behind the boulder after the impact when the boulder reaches equilibrium during a simulation; in the field-scale test, loose soil particles were able to fill the void created behind the boulder after impact when the boulder was rebounding. Nevertheless, Figure 11 and Figure 12 demonstrate

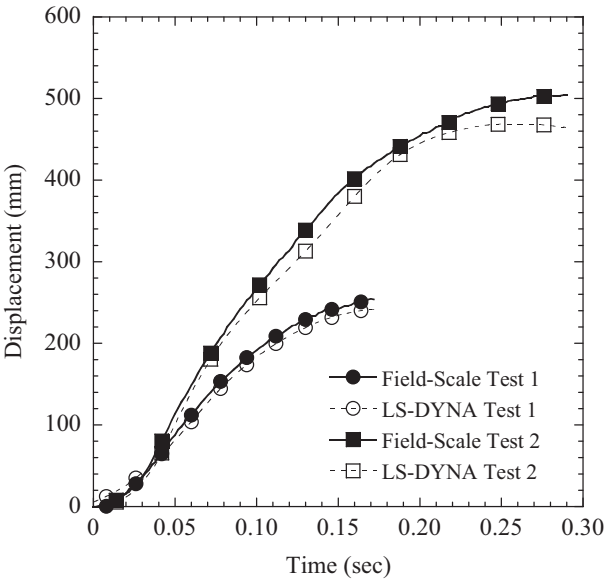

Figure 11. Center of gravity displacement for Tests 1 and 2

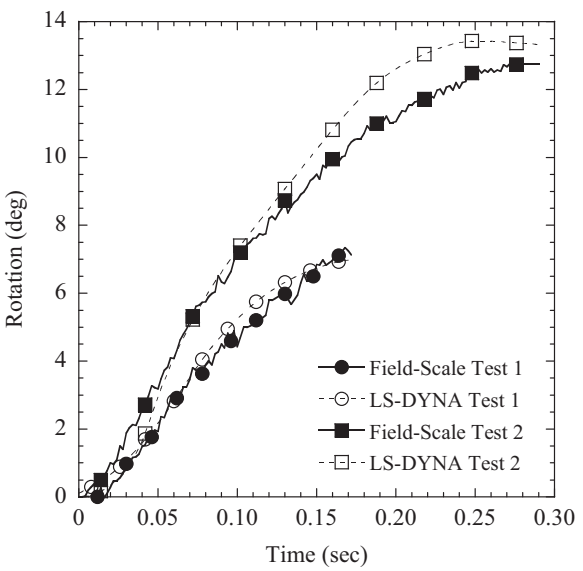

Figure 12. Center of gravity rotation for Tests 1 and 2

that LS-DYNA adequately captured the overall dynamic response of this LVAR system under vehicular impact. The calibrated soil properties also predicted the response of Test 2, which was rated for M50 as discussed previously.

Figure 13 shows the comparison of the simulated pressure-time histories at the location of the pressure cells with those recorded by the pressure cells for Test 1. Figure 14 shows the corresponding plot for Test 2.

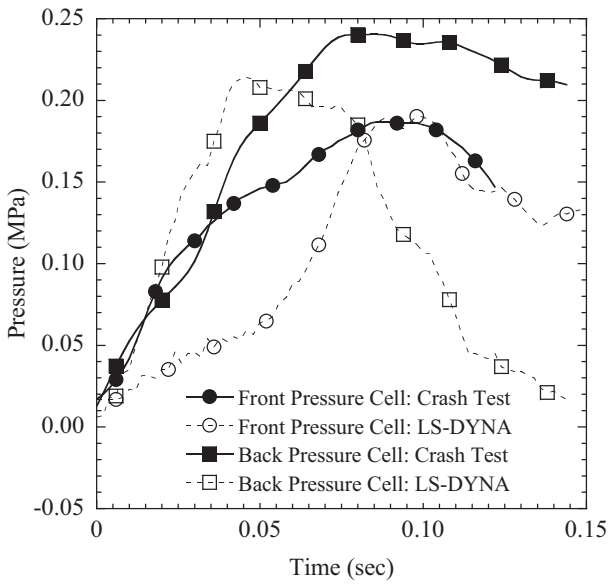

Figure 13. Pressure-time history comparison for Test 1 of field test and LS-DYNA

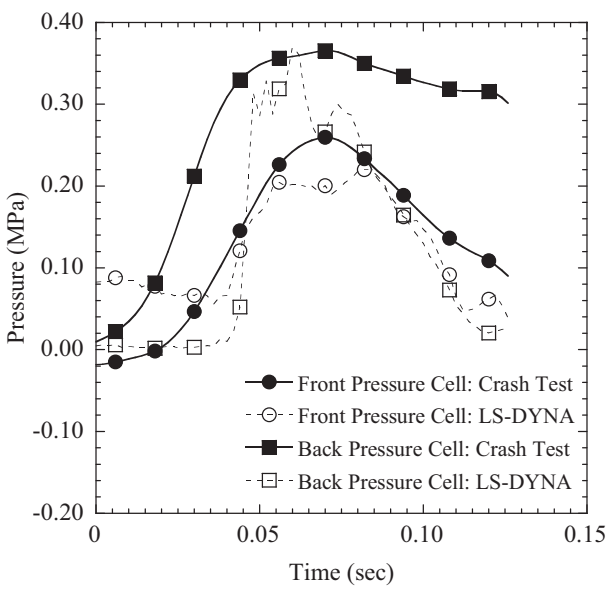

Figure 14. Pressure-time history comparison for Test 2 of field test and LS-DYNA

These figures show that the LS-DYNA model can capture the magnitude of the pressure experienced by the pressure cells during impact testing. In both figures, the simulated pressure-time history starts out at some value while the recorded pressure-time history starts near zero. This is attributed to the type of pressure cell used in the field-scale tests. The pressure cell only measures the change in pressure and has a zero reading at constant pressure, while the LS-DYNA simulations measure the pressure with respect to depth. The disparity between the simulated and recorded pressure-time histories might be due to a combination of several reasons. First, the effect of soil-pressure cell interaction in the field test was not considered in the LS-DYNA simulations since the pressure cells were not modeled. The simulated pressure-time histories in LS-DYNA were obtained by monitoring the pressure-time histories of the elements at the corresponding locations of the pressure cells. Second, the soil parameters were calibrated against the global response of Test 1, for which the response of the truck and boulder may have played a dominate role. Therefore, the calibrated soil parameters may not be able to accurately reflect the pressure-time history within the soil; however Figure 13 and Figure 14 indicate that the magnitudes of soil pressures were captured.

6. CONCLUSIONS

There is a lack of LVAR field-scale tests and corresponding numerical modeling to investigate the performance of these systems under vehicular impact. This paper presents two field-scale tests with corresponding LS-DYNA models to predict the global response of the system under vehicular impact. The LVAR system consisted of a single granite boulder embedded in AASHTO coarse aggregate subjected to M30 and M50 impact tests. Using high-speed cameras and pressure cells, information collected was used to calibrate both soil and boulder material parameters. This study suggests that: 1) a realistic truck model is imperative to accurately predict the global response of an LVAR system; and 2) using a simplistic material model for boulder and soil, LS-DYNA simulations were able to predict the global response such as boulder translational displacement and rotation during the impact events. Lastly, soil and boulder material properties calibrated based on the first test involving a vehicular impact at a lower speed were used to accurately predict the response of a second test involving a vehicular impact at a higher speed.

ACKNOWLEDGEMENTS

The authors would like to thank the United States Department of State and the Larson Transportation Institute at Pennsylvania State University for their continuing support of this research.

REFERENCES

[1] O'Hare, E., Linzell, D., Brennan, S., Rado, Z. Development of shallow foundation streetscape vehicular anti-ram (SVAR) systems through modeling and testing. *Proc 83rd Shock and Vibr* 2012. New Orleans, LA.

[2] Uzzolino, J., Veggeberg, K., Linzell, D. Testing anti-ram barrier protection systems at the Larson Institute Crash Safety Research Facility. *Proc 83rd Shock and Vibr* 2012. New Orleans, LA.

[3] Omar, T., Bedewi, N., Hylton, T. Cost-effective structural anti-ram security barriers – new design, computer modeling and test validation. *Proc ASME Int Mech Eng 2007*. Seattle, WA.

[4] Krishna-Prasad, B. Protective bollard design for high speed impact energy absorption. M.S. thesis. Wichita State University; 2006.

[5] Hu, B., Li, G., Chen, C., Shi, W. State-of-the-art review on anti-ram bollards. Key Eng Mat 2011; 90–93: 3206–13.

[6] Liu, C., Li, G., Phang, S.K., Sun, J. Effects of boundary conditions on the design of anti-ram bollards. Trans. Tianjin Univ. 2008; 14: 384–86.

[7] Ferdous, M., Akram, A-O., Bligh, R., Jones, H., Sheikh, N. Performance limit analysis for common roadside and median barriers using LS-DYNA. *Intl. J. of Crashworthiness* 2011; 16:6: 691–706

[8] Reese, L., Qiu, T., Linzell, D., Rado, Z., and Brennan, S. Development of landscape vehicular anti-ram systems through computational and experimental methods. *Proc 83rd Shock and Vibr* 2012. New Orleans, LA.

[9] U.S. Department of State. SD-STD-02.01. Specification for vehicle crash test of perimeter barriers and gates. 1985.

[10] American Society for Testing and Materials. F2656-07: Standard test method for vehicle crash testing of perimeter barriers. 2007.

[11] Briad J, Lim S, Bravo O, Alberson D, Abu-Odeh A, Arrington D, Mirdamadi A. Development of design guidelines for soil embedded post systems using wide-flange I-beams to contain truck impact. Summary Report: Texas Transportation Institute 2010.

[12] Hallquist, J.O. LS-DYNA keyword user's manual – version R7.0. Livermore Software Technology Corporation. Livermore, CA. 2013.

[13] Coldspring Quarry. Rockville White granite material properties. <http://www.coldspringusa.com/building-materials/products-colors-and-finishes/granite/rockville-white/>. January 7, 2014.

[14] Geokon, Inc. Instruction Manual – Models 4800, 4810, 4815, 4820, and 4830 VW Earth Pressure Cells. Lebanon, NH. 2011.

[15] Mohan, P., Marzougui, D., and Kan, S. Validation of a single unit truck model for roadside hardware impacts. *NCAC 2003-W-01*, The National Crash Analysis Center (NCAC), Ashburn, VA. 2003.

[16] National Crash Analysis Center (NCAC). Finite element model archive: Ford single unit truck, reduced model. 2008. <http://www.ncac.gwu.edu/vml/models.html>. September 3, 2013.

[17] Marzougui, D., Kan, C.D., and Opiela, K.S. Crash Test & Simulation Comparisons of a Pickup Truck & a Small Car Oblique Impacts Into a Concrete Barrier. *13th International LS-DYNA Users Conference* 2014. Dearborn, MI.

[18] Ray, M.H, Plaxico, C.A., and Anghileri, M. Procedures for Verification and Validation of Computer Simulations Used for Roadside Safety Applications. *NCHRP Web-Only Document 179*. 2010.

[19] Livermore Software Technology Company (LSTC). LS-DYNA Theory Manual. Livermore, CA. 2006.

[20] International Society for Rock Mechanics (ISRM). The Complete ISRM Suggested Methods for Rock Characterization, Testing and Monitoring: 1974–2006. 2007.

[21] Xia, K., Dai, F. and Chen, R. Split Hopkinson pressure bar tests of rocks: Advances in experimental techniques and applications to rock strength and fracture. *Advances in rock dynamics and applications*, Y. Zhou and J. Zhao, eds., CRC Press, London, UK. 2011. 35–77.

[22] Katz, O., Reches, Z., and Roegiers, J.-C. Evaluation of mechanical rock properties using a Schmidt Hammer. *International Journal of Rock Mechanics and Mining Services*. 2000. 37; 723–728.

[23] Gere, J. and Timoshenko, S. (1984). "Physical properties of building stone, brick and concrete." *Mechanics of Materials*, Brooks/Cole Engineering Division, Monterey, CA.

[24] Wyllie, D. and Mah, C. Rock strength properties and their measurement. *Rock Slope Engineering: Civil and Mining*, Spon Press, New York, NY, 2004. 74–109.

[25] Bolton, M. The strength and dilatancy of sands. *Geotechnique* 36, 1, 1986. 65–78.

[26] Das, B. Principle of Foundation Engineering 7th Edition. Cengage Learning, Stamford, CT.